

Heating liquid dielectrics by time dependent fields

A. Khalife, U. Pathak, and R. Richert^a

Department of Chemistry and Biochemistry, Arizona State University, Tempe, 85287-1604 Arizona, USA

Received 21 July 2011 / Received in final form 6 September 2011

Published online 17 October 2011 – © EDP Sciences, Società Italiana di Fisica, Springer-Verlag 2011

Abstract. Steady state and time-resolved dielectric relaxation experiments are performed at high fields on viscous glycerol and the effects of energy absorption from the electric field are studied. Time resolution is obtained by a sinusoidal field whose amplitude is switched from a low to a high level and by recording voltage and current traces with an oscilloscope during this transition. Based on their distinct time and frequency dependences, three sources of modifying the dynamics and dielectric loss via an increase in the effective temperature can be distinguished: electrode temperature, real sample temperature, and configurational temperatures of the modes that absorbed the energy. Isothermal conditions that are desired for focusing on the configurational temperature changes (as in dielectric hole burning and related techniques) are maintained only for very thin samples and for moderate power levels. For high frequencies, say $\nu > 1$ MHz, changes of the real temperature will exceed the effects of configurational temperatures in the case of macroscopic samples. Regarding microwave chemistry, heating via cell phone use, and related situations in which materials are subject to fields involving frequencies beyond the MHz regime, we conclude that changes in the configurational (or fictive) temperatures remain negligible compared with the increase of the real temperature. This simplifies the assessment of how time dependent electric fields modify the properties of materials.

1 Introduction

Dielectric relaxation experiments performed at electric fields that take the sample beyond the regime of linear responses can provide information that is not available from their low field counterparts [1–4]. Dielectric saturation is one example for which the polarization magnitude remains below the linear field dependence because the dipole orientation has an upper limit given by $\langle \cos \theta \rangle \leq 1$ [5]. Another nonlinear effect stems from the energy the sample can absorb from the external field at sufficiently high fields [6]. It is generally recognized that dielectric relaxation experiments involve a power density p with which energy is transferred irreversibly to the sample. According to Joule's law, the power density p absorbed is the field E times the in-phase component $\sigma' E$ of the current density j ,

$$p \propto \sigma' |E|^2 = \omega \varepsilon_0 \varepsilon'' |E|^2 = \omega \varepsilon_0 \varepsilon' \tan \delta |E|^2, \quad (1)$$

where σ' is the real part of the conductivity $\hat{\sigma}(\omega) = \sigma' + i\sigma''$ [7]. The power density can also be expressed in terms of the loss component ε'' of the dielectric function $\hat{\varepsilon}(\omega) = \varepsilon' - i\varepsilon''$ or via the loss tangent, $\tan \delta = \varepsilon''/\varepsilon'$. In this context, the typical assumption is that the amount of energy involved is marginal and insufficient for modifying the dielectric behavior of the sample. On the other hand, external electric fields are exploited to heat chemicals or food as in a microwave oven [8–10], a situation

which clearly drives the sample beyond its linear regime in which the sample properties remain unchanged and polarization is proportional to the field amplitude.

The idea that irreversible energy transfer will modify mainly the mode that absorbed it has been used in non-resonant hole-burning experiments to study the heterogeneous aspect of dynamics that is particularly pronounced for glass-forming liquids in their viscous regime [1,11–13]. Such supercooled liquids are known to display a distribution of relaxation times in their (linear) susceptibilities [14,15]. If these faster and slower modes (or dynamically distinct domains) are relaxing independently [16,17], then energy absorbed selectively in a certain spectral region will not have the same effect as an increase in the macroscopic real temperature [6,11]. Dielectric hole-burning has demonstrated that the non-exponential character of the overall relaxation originates from a superposition of exponential modes which relax highly independently regarding both polarization and enthalpy content [18,19]. Non-linear impedance techniques have also been employed to study the conductivity at high fields [20,21]. A more recent application of dielectric relaxation experiments in the non-linear regime is based upon a theory that links the (third order) non-linear susceptibility to the number of particles that are dynamically correlated [22].

While a dielectric is exposed to a time dependent field, the system is generally not in equilibrium and the bath temperature alone is no longer sufficient for defining the

^a e-mail: ranko@asu.edu

state and behavior of the material. In order to appreciate the difference between standard heating and the effect of energy absorption from a field, one has to realize that a time dependent field does work on the dipolar degrees of freedom of a dielectric, and only eventually is this energy converted to heat and measurable as a temperature increase. The energy absorbed by a dielectric can modify the dynamics of the system via different effects: either by elevating the fictive temperatures (configurational temperatures, dipole temperatures) of the modes that are involved in the absorption process, or by a change in the real measurable temperature, or both. Non-linear dielectric experiments such as the hole burning approach focus on the changes of the fictive temperature, and these experiments are designed to maintain isothermal conditions [23,24]. In the case of microwave chemistry or the use of a household type microwave oven, it is obviously the elevation of the real temperature that is targeted. In this paper, we investigate the magnitudes of changes regarding fictive and real temperatures in high field impedance measurements. It is demonstrated that the sample thickness plays an important role, and that fictive and real temperature effects can be discriminated experimentally. The experiments indicate that Joule heating and thermal diffusion to the electrodes (that are considered thermostats) can underestimate the increase in real temperature. The implications regarding microwave chemistry and heating via cell phone use are discussed.

2 Experiments and analysis

2.1 Materials

The main material used for this study is the polar glass-forming liquid glycerol (99.5 + %, spectrophotometric grade), which has been used as received. The water concentration is 710 ± 20 ppm, as determined previously using Karl Fischer titration [25]. Other liquids involved in this study are propylene glycol (1,2 propanediol, 99.5+ %), methanol (99.9%, spectrophotometric grade), and water (HPLC grade). All chemicals are purchased from Aldrich.

2.2 Steady state impedance

The impedance for frequencies between 1 Hz and 50 kHz is measured by a Solartron SI-1260 gain/phase analyzer, with the generator voltage amplified using a Trek PZD-700 high-voltage amplifier. The voltage at the sample is recorded via input V1 of the SI-1260 using the voltage monitor output of the amplifier, the current is recorded via input V2 as the voltage drop across a 100 Ω resistor. A voltage follower protects the SI-1260 V2 input against high voltages in case of a sample failure. This circuit is based upon the AD-549L operational amplifier [26], and protects against 300 V. The finite bandwidths of both the high voltage and the buffer amplifiers are accounted for by reference measurements with virtually loss free capacitors. Sinusoidal electric fields, $E(t) = E_0 \sin(\omega t)$, with

zero dc offset are applied to the sample. The SI-1260 is programmed to apply the high voltage for about 30 ms, with only the final 20 ms being used for data acquisition and analysis in order to suppress transient effects. This sequence is followed by a much longer cooling time at zero-field, and then the lower voltage measurement using $E_0 = 14$ kV/cm is performed. All field induced changes obtained in this manner are entirely reversible. These measurements were performed using a Novocontrol *l*-N₂ cryostat with Quatro controller.

2.3 Time-resolved technique

For the time resolved measurements, liquid samples are prepared between two polished stainless steel electrodes (16 mm and 20 mm diameter), separated by a Teflon ring of 10 μ m thickness with 14 mm inner and 20 mm outer diameter that covers the electrode edge. One electrode is spring loaded to maintain a temperature invariant stress on the Teflon ring. The cryostat used for temperature control of the sample cell is a Leybold RDK 6-320/Coolpak6200 closed-cycle helium refrigerator with Lakeshore Mod. 340 controller equipped with calibrated DT-470-CU diode sensors.

The applied voltage originates from a programmable function generator (SRS DS-345) and a digitizing oscilloscope (Nicolet Sigma 100) records voltage across and current through the sample (using a shunt of order $R = 1$ k Ω). The technique facilitates changing the field amplitude from one period to the next and to monitor the changes with a period-by-period time resolution. The amplitude change by a factor of 5 is under the control of an arbitrary amplitude function that is cycled at a give repetition rate. In this manner, the transition from low to high voltage and back can be programmed without limitation on the number of cycles associated with high fields, but the amplitude transition does not necessarily coincide with the beginning of a period. Repetition rates of order $r = 0.1$ Hz are used, implying that the high field duty cycle remains small (≤ 0.1) and the sample is given ample time to equilibrate between energy absorption intervals. The oscilloscope can average over up to 5000 repeated signals, so that a resolution of up to 5×10^{-5} regarding $\tan \delta$ for a particular period is achieved.

The two signals, voltage $V(t)$ and current $I(t)$, are subject to period-by-period Fourier analysis according to

$$R = \frac{\omega}{\pi} \int_0^{2\pi/\omega} \sin(\omega t) S(t) dt = A \cos(\varphi),$$

$$I = \frac{\omega}{\pi} \int_0^{2\pi/\omega} \cos(\omega t) S(t) dt = A \sin(\varphi), \quad (2)$$

where $S(t) = V(t)$ or $S(t) = I(t)$ for analyzing voltage or current, respectively. The amplitude is obtained by $A = \sqrt{R^2 + I^2}$ and the phase by $\varphi = \arctan(I/R)$. For each of the 1000 to 4000 periods measured in one frame,

this defines V_0 , φ_V , I_0 , and φ_I with respect to the notation $V(t) = V_0 \sin(\omega t + \varphi_V)$ and $I(t) = I_0 \sin(\omega t + \varphi_I)$. The loss tangent, $\tan \delta$, turns out to be the most robust quantity for measuring how energy absorption modifies the dynamics of the system, and its value is determined using $\tan \delta = \tan(\pi/2 - \varphi_V + \varphi_I)$. These techniques facilitate monitoring the time-evolution of the field induced changes after applying or removing the high electric field. Although the system is generally not in equilibrium during these measurements, we continue to use notations such as $\tan \delta$, ε' , and ε'' that are actually meant to reflect equilibrium situations.

The code performing the Fourier analysis also evaluates the power transferred irreversibly to the sample,

$$P = \overline{VI} = \frac{1}{2} V_0 I_0 \cos(\varphi_I - \varphi_V) = \frac{1}{T} \int_t^{t+T} V(t) I(t) dt. \quad (3)$$

We chose the VI -integration approach because this is correct also in the case of deviations from pure harmonic signals. Additionally, the permittivity and loss are computed via

$$\varepsilon'(\omega) = \frac{I_0 \sin(\varphi_I - \varphi_V)}{V_0 \omega C_{geo}}, \quad \varepsilon''(\omega) = \frac{I_0 \cos(\varphi_I - \varphi_V)}{V_0 \omega C_{geo}}, \quad (4)$$

so that consistency with standard impedance results, $\hat{\varepsilon}(\omega) = \varepsilon'(\omega) - i\varepsilon''(\omega)$, can be verified. Here, $C_{geo} = \varepsilon_0 A/d$ is the geometric capacitance, with ε_0 representing the permittivity of vacuum, A is the sample area, and d the electrode separation or sample thickness.

3 Results

In what follows, the high field effects are analyzed as the difference in either the loss ε'' or loss factor $D = \tan \delta$ between the high field results and their low field limit counterparts, i.e., $\Delta \varepsilon'' = \varepsilon''(E_0 \gg 0) - \varepsilon''(E_0 \rightarrow 0)$ or $\Delta \tan \delta = \tan \delta(E_0 \gg 0) - \tan \delta(E_0 \rightarrow 0)$. As the relative changes are more relevant, we present data as $\Delta \ln(\varepsilon'') = \Delta \varepsilon''/\varepsilon''$ and $\Delta \ln(\tan \delta) = \Delta \tan \delta/\tan \delta$. Frequency resolved $\Delta \ln \varepsilon''$ data for propylene glycol at $T = 194$ K are shown in Figure 1. The two curves differ in the electrode spacing d used, $32 \mu\text{m}$ versus $10 \mu\text{m}$, but the high electric field has been $E_0 = 132.6$ kV/cm in both cases. The $32 \mu\text{m}$ case does not only show a more pronounced field effect but also lacks the leveling off seen for the $10 \mu\text{m}$ data at frequencies $\nu > 3$ kHz. Analogous results are observed for glycerol, a mixture of 33 wt% water in glycerol, and a mixture of 33 wt% methanol in glycerol (not shown). All field induced effects are proportional to the square of the applied field, i.e. $\Delta \ln(\varepsilon'') \propto E_0^2$.

The time resolved field effects have all been measured on glycerol at $T = 207$ K. For this situation, the spectra for dielectric loss ε'' and loss factor $\tan \delta$ are shown in Figure 2. This graph includes the frequency positions of the time resolved experiments which are indicated by arrows. A typical result of the time resolved field effect

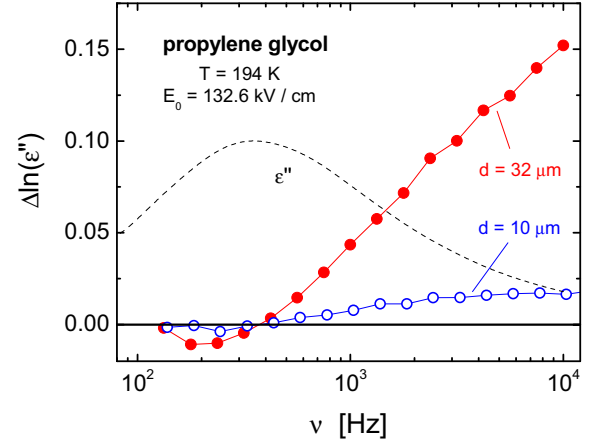


Fig. 1. (Color online) Relative change of the dielectric loss, $\Delta \ln(\varepsilon'')$, at a field of 132.6 kV/cm with respect to the low field counterpart for propylene glycol at $T = 194$ K. Solid symbols are for an electrode spacing of $d = 32 \mu\text{m}$, open symbols for a sample thickness of $d = 10 \mu\text{m}$. While the $10 \mu\text{m}$ data develops a plateau for $\nu > 3$ kHz, the ε'' values for the $32 \mu\text{m}$ case rises continuously with frequency. The low field loss spectrum (scaled arbitrarily) is represented by the dashed line and shows a peak at $\nu_{max} \approx 300$ Hz.

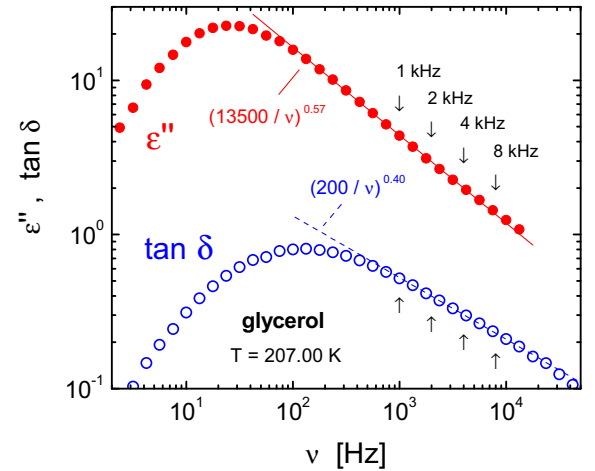


Fig. 2. (Color online) Dielectric loss (ε'' , solid symbols) and loss tangent ($\tan \delta$, open symbols) for glycerol at $T = 207$ K. The lines represent the power laws approximating the high frequency slopes, $\varepsilon'' = (13500/\nu)^{0.57}$ and $\tan \delta = (200/\nu)^{0.40}$. The arrows indicate the measurement frequency positions of the time resolved experiments.

experiments is depicted in Figure 3, where the upper data set represents the original values for $\tan \delta$ as measured. In essence, this is a four point correlation function, two points in time regarding polarization (defined by the measurements frequency of 8 kHz), and two points in time regarding the onset of energy transfer (at $t = 0$). Following earlier reasoning, we assume that the final linear increase of $\Delta \ln(\tan \delta)$ with time is due to a temperature increase of the electrodes. In order to justify this assignment, this slope $S = d\Delta \ln(\tan \delta)/dt$ is evaluated for times $t \gg 0$ for different frequencies ν , sample thicknesses d , and electric

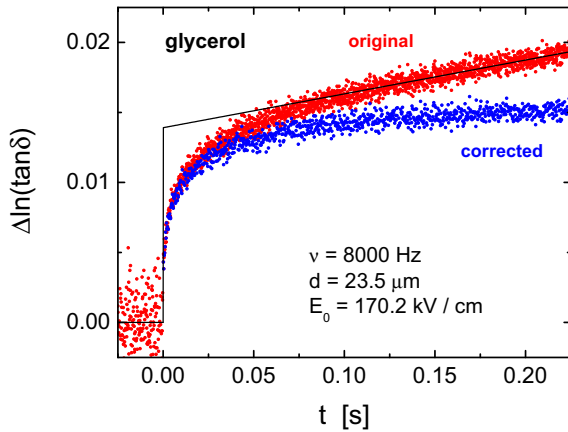


Fig. 3. (Color online) Time resolved field induced relative change of the loss tangent, $\Delta \ln(\tan \delta) = \Delta \tan \delta / \tan \delta$ for glycerol at $T = 207$ K measured at $\nu = 8$ kHz. The electric field was increased from $E_0 = 34$ kV/cm to 170 kV/cm at $t = 0$ by increasing the voltage across the $d = 23.5$ μm sample by a factor of 5. The upper data set labeled ‘original’ is as measured and displays a constant slope for $t > 0.1$ s. The lower data is corrected for this temperature drift of the electrodes via subtracting the linear fit, $y = H + Sx$, represented by the solid line, for $t > 0$.

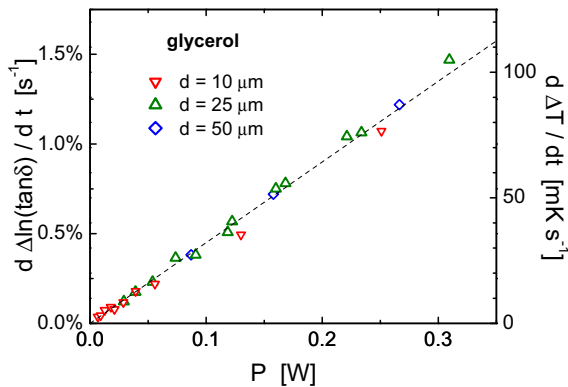


Fig. 4. (Color online) Slopes $S = d\Delta \ln(\tan \delta)/dt$ as indicated in Figure 2 versus power P for different samples of glycerol at $T = 207$ K. Power levels in the range of 6.7 to 310 mW have been achieved by varying electrode distances (10 to 50 μm), frequency (1 to 8 kHz), and electric fields (57 to 270 kV/cm). The dashed line reflects a fit $dT/dt = p/C_p$ with $C_p = 3.1$ J/K.

field amplitudes E_0 . An example for a linear fit leading to such a slope is included as line in Figure 3. For each case, the power P is evaluated, and Figure 4 compiles the results $S(P)$ from 22 separate measurements at two different nominal distances, $d = 10$ μm and 25 μm .

With the long time slopes S evaluated, we proceed to subtract the linear relation $S \times t$ for $t > 0$ from the time resolved $\Delta \ln(\tan \delta)$ data, resulting in curves that become level at long times. Figure 3 displays an example of this correction (lower data), now equivalent to the situation of isothermal electrodes. By averaging over the long time values of these corrected curves, we obtain the steady state field-induced change of $\tan \delta$ under constant

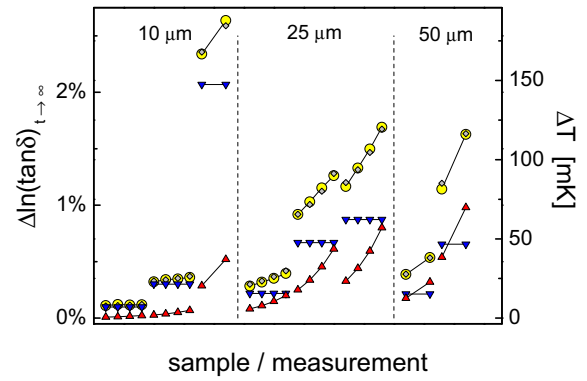


Fig. 5. (Color online) Experimental results (circles filled yellow) for the steady state field induced relative change of $\tan \delta$, derived from the time resolved curves after correcting for the electrode temperature drift (see Fig. 3). The abscissa serves only to separate distinct measurements, which are separated in terms of the nominal electrode distance d , as indicated. For each d , data are sorted by the field amplitude E_0 . Values with a common d and E_0 are connected by lines and differ only in the frequency ν . Within each connected set, points are uniformly spaced along the abscissa regarding $\log(\nu)$. The calculated fictive and real temperature effects are shown as triangles pointing down (blue) and up (red), respectively. The sum of these two effects is represented by small diamonds (grey).

electrode temperature conditions. These heights are compiled in Figure 5 (larger circles), with the abscissa axis simply separating distinct measurements. The measurements are sorted by nominal sample thickness d as indicated, and then by the field amplitude E_0 used. A set of data with common d and E_0 is connected by a line and values within such a set differ only in the frequency ν .

4 Discussion

The results presented in the previous section indicate field induced increases regarding ε'' or $\tan \delta$ with relative changes between 0.1% and 15%. As emphasized before [1,11,18,24], these modifications in $\varepsilon^*(\omega)$ are the signature of reduced relaxation time constants τ , because the dynamics are much more sensitive than the dielectric constant ε_s to temperature changes. While this suggests non-linear behavior of these samples, one would not expect a dependence on sample dimensions on the basis of the typical non-linear dielectric effects [24]. Field effects of a similar magnitude have been observed in dielectric hole burning and similar high field studies where energy absorption is at the origin of the non-linear dielectric effect [6,18,19]. Dielectric hole burning was originally performed with the intent to assess the heterogeneous nature of relaxations in supercooled liquids [16,17]. The basic idea is that the impact of energy absorption from an external field should depend on its frequency if the relaxation time dispersion is the result of dynamically distinct domains which relax quite independently. If a system is heterogeneous in this sense, then different high field frequencies

will let different modes absorb the bulk of the field energy, and the dielectric loss will be subject to a change in a spectrally selective fashion. It is only for the thin samples and moderately high fields that the present results are entirely consistent with the previous high field dielectric studies [2].

A brief outline of the steady state effect of energy absorption appears in order, with details and time dependent effect having been discussed in depth elsewhere [6,13,18,23,24]. For a material with dielectric loss ε'' subject to a sinusoidal field with peak amplitude E_0 , the amount of energy irreversibly transferred from the field to the sample is given by the power density $p = \varepsilon_0 E_0^2 \varepsilon'' \omega / 2$, but the energy does not enter the sample as heat. Instead, the field does work on the dipoles, which only eventually will be converted to heat and an increase in the (measurable) bath temperature. Initially, the enthalpy content of the slow degrees of freedom is elevated for those modes that have a relaxation time that matches approximately the frequency of the applied field. This elevated enthalpy content can be expressed in terms of a net increase in the fictive temperature of the mode in question, and a concomitant decrease of its relaxation time constant. A shift of a time constant, in turn, affects the profile of ε'' and $\tan \delta$ at a given frequency. In steady state conditions, each domain establishes a balance between a gain in configurational temperature $dT_{cfg} = +P\rho^{-1}C_p^{-1}dt$ and a loss via enthalpy relaxation of magnitude $dT_{cfg} = -(T_{cfg} - T)\tau^{-1}dt$ [2,24]. Therefore, the configurational temperature of a mode will eventually settle at

$$T_{cfg} = T + \frac{\varepsilon_0 E_0^2 \Delta\varepsilon}{2\rho\Delta C_p}. \quad (5)$$

Within the framework of this model, the volume fraction or weight (g_i) of a mode i does not enter this equation, because it affects the value of the dielectric loss ($g_i\Delta\varepsilon$) and of the heat capacity ($g_i\Delta C_p$) equally for each mode or domain, and the g_i thus cancel [13]. If the frequency ω of the external field is increased, the rate of enthalpy gain increases but the rate of enthalpy relaxation for a mode with $\tau = 1/\omega$ accelerates equally, and the net effect remains the same. As a consequence, the steady state prediction for T_{cfg} is as simple as equation (5), which has been verified by experiment [2,24].

Regardless of the source of a temperature increase, T_{cfg} or the real temperature T , the effect on the relaxation time constant τ is given by the activation parameter $d\ln\tau/dT = -0.35 \text{ K}^{-1}$ for glycerol near 207 K, and the effect on ε'' further involves the slope $d\ln\varepsilon''/d\ln\omega = -0.57$ (-0.40 for $\tan\delta$). As demonstrated in Figure 2, these slopes are practically constant in the 1 to 8 kHz range of current interest. Using an earlier strategy for determining the real electrode distances from the measured permittivity¹, the expected steady state values for $\Delta\ln(\tan\delta)$ have

¹ This involves comparing the results against a reference measurement of the same material but with negligible distance uncertainty. First $\tan\delta$ is checked to ensure the capacitor is completely filled, then the level of ε is compared with the reference to infer the actual geometry [19].

been calculated and included in Figure 5 as lower set of triangles pointing down (blue). Obviously, this does not explain the observed field effects, with the exception of the lowest field set of four points with $d = 10 \mu\text{m}$.

As the slow degrees of freedom absorb energy, the same amount of energy is eventually passed on as heat to the vibrational modes, which account for approximately half of the heat capacity of a liquid [27]. This will lead to an increase of the real sample temperature, unless this heat is conducted effectively to the electrodes. The metal electrodes are expected to act as thermostats, as their heat capacities are large compared with that of the sample material. However, applying high fields for an extended period of time does lead to a slow linear increase of $\Delta\ln(\tan\delta)$ with time, as seen in Figure 3. For power levels ranging from 6.7 to 310 mW, this slope is linear in the power (see in Fig. 4) and otherwise not dependent on electrode separation, frequency, or electric field. The dashed line in Figure 4 represents a fit according to $dT/dt = p/C_p$ with $C_p = 3.1 \text{ J/K}$, consistent with the amount of iron used for the electrodes. Therefore, the long time linear $\Delta\ln(\tan\delta)$ versus t effect is clearly a result of electrode heating, and after correcting for these slopes we can quantify the effects that had been obtained if the electrodes were perfect cryostats and maintained a constant temperature.

For the case of constant electrode temperatures, the net heating effect can be calculated on the basis of the thermal diffusion equation with a spatially uniform heat source, which for steady state conditions, $\partial\Delta T(z)/\partial t = 0$, reads

$$\frac{\partial^2 \Delta T(z)}{\partial z^2} = -\frac{p}{\kappa}, \quad (6)$$

where ΔT refers to the temperature increase relative to the electrode and cryostat temperature. Because the lateral dimensions are large compared with d , the direction z normal to the electrodes is the only spatial dimension of interest. The clamped electrode temperatures enter the calculation as boundary conditions, $\Delta T(z=0) = \Delta T(z=d) = 0$. The solution is $\Delta T(z) = (zd - z^2)p/2\kappa$, and for the average temperature increase we obtain by integration

$$\Delta T_{avg} = \frac{1}{d} \int_0^d \Delta T(z) dz = \frac{pd^2}{12\kappa} = \frac{\varepsilon_0 \varepsilon'' E_0^2 \omega d^2}{24\kappa}. \quad (7)$$

The highest value of ΔT occurs at the center ($z = d/2$) and amounts to $\Delta T_{max} = 1.5\Delta T_{avg}$.

In contrast to the configurational temperature result, T_{cfg} of equation (5), the real heating effect of equation (7) depends explicitly on frequency ω . Therefore, this contribution has the potential to account for the measured frequency dependence of $\Delta\ln(\tan\delta)$ seen in Figure 5, recalling that only the frequency is varied within a set of connected symbols. Testing this hypothesis reveals that equation (7) accounts only for a fraction of the frequency effect when the thermal conductivity of glycerol at $T = 207 \text{ K}$, $\kappa = 0.29 \text{ W K}^{-1} \text{ m}^{-1}$ [28], is used in equation (7). Establishing agreement with the data can be achieved, however, by a lower value for κ that is adjusted for each sample. For the samples with actual electrode distances

$d = 10.8, 14.0, 23.5,$ and $47.5 \mu\text{m}$ the respective values $\kappa_{\text{eff}} = 0.04, 0.10, 0.07,$ and $0.13 \text{ WK}^{-1} \text{ m}^{-1}$ generate coincidence with the observed effects, as demonstrated in Figure 5. Although these effective values for κ differ considerably from the true κ value for glycerol, an important observation is that only a single κ_{eff} is needed for each sample and the κ_{eff} tends to approach κ of glycerol for the thicker samples. A realistic explanation is that a considerable thermal contact resistance at the glycerol/metal interface exists, which is not reproduced for subsequent sample preparations. A comparison with the thermal calibration outlined by Minakov et al. [28] reveals that their glycerol/metal contact resistance is of comparable magnitude.

One obvious consequence of the above thermal contact resistance observation is that sample dimensions below $100 \mu\text{m}$ are inappropriate for measuring the thermal conductivity of viscous organic liquids. For the measurement of configurational temperature effects, however, the results imply that sample thicknesses in excess of $10 \mu\text{m}$ will fail to maintain isothermal condition. Due to the thermal resistances at the electrode interface, the temperature effect calculated via thermal diffusion will tend to underestimate the increase of the real temperature, a problem which becomes more pronounced as the power is increased. An inspection of Figure 5 shows that the frequency invariance of the magnitude of $\Delta \ln(\tan \delta)$ that is characteristic of the configurational temperature model described above is lost already for moderate fields or powers when $d > 10 \mu\text{m}$. For instance, the higher field set of 4 frequencies at $d = 10 \mu\text{m}$ already displays a frequency dependence that amounts to an excess temperature of 3 mK at 8 kHz over the 1 kHz case. In conclusion, thicker samples will show a more pronounced field effect for which the trivial heating contribution is easily underestimated, because a temperature step exists across the sample/electrode interfaces.

Finally, we address the implications of these observations on microwave chemistry [8,9], and the heating effects during the exposure of tissue material to microwave electromagnetic radiation (as in cell phone use) [29,30]. In microwave chemistry, a 2.45 GHz radiation source is used instead of a hotplate or oil bath to elevate the temperature of a reaction medium [8,9]. Similar to the present experiments, the external electric field does work on the charges, and both configurational and real temperatures will be affected. The lower frequency high field dielectric experiments clearly demonstrate that time dependent fields are capable of accelerating molecular mobility and perhaps reactivity without changing the true temperature of the sample. The present results, however, demonstrate that such non-equilibrium features are significant only for relatively low frequencies and samples that are thin compared with the thermal wavelength, $\lambda = \sqrt{\kappa/(\omega\rho C_p)}$, of the system. It simplifies the assessment of the effects of external fields regarding the net temperature effects, as only the real temperature needs to be considered, which is measurable in principle. Of course, local heating can occur in cases where absorptivity is a spatially varying quantity.

In this situation the magnitude of the temperature gradients that occur will depend on the power gradients and thermal conductivity. Such local heating effects will be difficult to detect experimentally, and in complex systems this may lead to effects that are more pronounced than what is expected on the basis of the macroscopically averaged temperature. Conversely, energy may be deposited in a material in a more targeted manner with the correct choice of the frequency, which is impossible in the case of standard heating techniques.

5 Summary and conclusions

Heating a dielectric by time dependent fields tends to generate fictive temperatures of the absorbing modes that are elevated above the true bath temperature. The net temperature effects are studied by time-resolved high field dielectric relaxation experiments, which allowed us to quantify the changes of the configurational, real sample, and electrode temperatures. The results demonstrate that the impact of ‘configurational heating’ is significant only for low frequencies of the electric field and samples that are thermally clamped to a thermostat (metal electrodes) in a very effective manner. For heating macroscopic samples with fields in the microwave frequency range, we conclude that any disparities between configurational and real bath temperature are negligible, unless a mode is involved that can absorb energy at a rate much faster than its equilibration with the bath. In other words, the non-equilibrium effects of fictive temperatures that exceed the real temperature do not seem important in the context of microwave heating. This should be considered a simplification regarding understanding the difference between conventional and microwave heating and the effects of cell phone radiation on tissue material.

This material is based upon work supported by the National Science Foundation under Grant No. CHE-1026124 (International Collaboration in Chemistry).

References

1. B. Schiener, R. Böhmer, A. Loidl, R.V. Chamberlin, *Science* **274**, 752 (1996)
2. R. Richert, S. Weinstein, *Phys. Rev. Lett.* **97**, 095703 (2006)
3. J. Malecki, *J. Mol. Struct.* **436-437**, 595 (1997)
4. C. Brun, C. Crauste-Thibierge, F. Ladiou, D. L'Hôte, *J. Chem. Phys.* **134**, 194507 (2011)
5. A. Piekara, A. Chelkowski, *J. Chem. Phys.* **25**, 794 (1956)
6. B. Schiener, R.V. Chamberlin, G. Diezemann, R. Böhmer, *J. Chem. Phys.* **107**, 7746 (1997)
7. H. Fröhlich, *Theory of Dielectrics* (Clarendon, Oxford, 1958)
8. S.A. Galema, *Chem. Soc. Rev.* **26**, 233 (1997)
9. D. Dallinger, C.O. Kappe, *Chem. Rev.* **107**, 2563 (2007)

10. C. Gabriel, S. Gabriel, E.H. Grant, B.S.J. Halstead, D.M.P. Mingos, *Chem. Soc. Rev.* **27**, 213 (1998)
11. K.R. Jeffrey, R. Richert, K. Duvvuri, *J. Chem. Phys.* **119**, 6150 (2003)
12. T. Blochowicz, E.A. Rössler, *J. Chem. Phys.* **122**, 224511 (2005)
13. K. Duvvuri, R. Richert, *J. Chem. Phys.* **118**, 1356 (2003)
14. M.D. Ediger, C.A. Angell, S.R. Nagel, *J. Phys. Chem.* **100**, 13200 (1996)
15. C.A. Angell, K.L. Ngai, G.B. McKenna, P.F. McMillan, S.W. Martin, *J. Appl. Phys.* **88**, 3113 (2000)
16. M.D. Ediger, *Annu. Rev. Phys. Chem.* **51**, 99 (2000)
17. R. Richert, *J. Phys.: Condens. Matter* **14**, R703 (2002)
18. S. Weinstein, R. Richert, *Phys. Rev. B* **75**, 064302 (2007)
19. L.-M. Wang, R. Richert, *Phys. Rev. Lett.* **99**, 185701 (2007)
20. B. Roling, *J. Chem. Phys.* **117**, 1320 (2002)
21. R. Richert, R. Böhmer, *Phys. Rev. Lett.* **83**, 4337 (1999)
22. C. Crauste-Thibierge, C. Brun, F. Ladieu, D. L'Hôte, G. Biroli, J.-P. Bouchaud, *Phys. Rev. Lett.* **104**, 165703 (2010)
23. W. Huang, R. Richert, *J. Phys. Chem. B* **112**, 9909 (2008)
24. W. Huang, R. Richert, *J. Chem. Phys.* **130**, 194509 (2009)
25. R. Richert, *J. Chem. Phys.* **133**, 074502 (2010)
26. *Analog Devices, Datasheet for AD549, rev. F* (2006), p. 13
27. W. Kauzmann, *Chem. Rev.* **43**, 219 (1948)
28. A.A. Minakov, S.A. Adamovsky, C. Schick, *Thermochim. Acta* **403**, 89 (2003)
29. M. Kundi, *Environ. Health Persp.* **117**, 316 (2009)
30. P.W. French, R. Penny, J.A. Laurence, D.R. McKenzie, *Differentiation* **67**, 93 (2000)